Acoustic Impedance and the Control of Sound Waves

Lixi Huang

Abstract Acoustic impedance is one of the most important parameters for fluid media and is determined by effective mass and elastic modulus. For an acoustic absorber with a shallow depth, the system has high characteristic resonance frequency and its performance is controlled by the system stiffness which is inversely proportional to the depth. This study begins with the analysis of a common porous material as the benchmark and compares with the traditional micro-perforated panels (MPP) before introducing advanced designs. It is shown that MPP can indeed yield similar performance as the porous material when the aperture is very small hence high cost. However, the performance at very low frequencies remains poor. In order to achieve a broadband performance, parallel resonator array is required. This system is shown to reduce system stiffness significantly while the overall mass increase is much smaller than that of a single MPP resonator. Advanced means of reducing system stiffness by electromagnetic forces is discussed, and the physics of a negative dynamic mass is also analyzed.

1 Introduction

Control of sound waves takes two forms, wave reflection and absorption. The latter is more preferable but is harder to achieve at low frequencies. One important application of acoustics is the control of environmental noise which often features heavy low-frequency contents which also spread over a broad frequency band (measured by the ratio of high-to-low frequency limits). For instance, the limits of 100 Hz–1 kHz are used in the examples given in the current study as noise absorption above 1 kHz is easy in existing technology.

L. Huang (✉)
Lab for Aerodynamics and Acoustics, Department of Mechanical Engineering, Zhejiang Institute of Research and Innovation, The University of Hong Kong, Hong Kong, China
e-mail: lixi@hku.hk

Y. Zhou et al. (eds.), *Fluid-Structure-Sound Interactions and Control*, Lecture Notes in Mechanical Engineering,
https://doi.org/10.1007/978-981-10-7542-1_48

The most traditional noise absorber is, of course, the porous sound absorption material (henceforth SAM) which is typically made of glass fiber or rockwool. Porous materials easily accumulate dusts and they may not be acceptable when considerations of hygiene are crucial. Micro-perforated panels (MPP) are used instead as panels are easily cleansed and they are esthetically more appealing. However, the traditional use of MPP is limited to a single resonator formed between the panel and the back cavity. Sound absorption is limited only to a narrow frequency band around the resonance frequency. In what follows, the next section gives a brief review of these with the help of a set of lumped parameters of system mass, resistance and stiffness. Using the concept of system mass and stiffness, the superior performance of the parallel array of MPP resonators is quantified, and the concepts of negative dynamic mass and negative stiffness are also introduced.

2 Reference Absorber and System Parameters

Figure 1a shows the configuration of sound absorption by a layer of SAM with thickness h. For simplicity the study is limited to normal incident sound although the results are easily extended to oblique and random incidence. Figure 1b, 1c illustrate the absorber made of MPPs in series and parallel arrangements, which are discussed in this and next sections, respectively.

Textbook formulation gives the following sound energy absorption coefficient

$$\alpha = 1 - \left|\frac{Z-1}{Z+1}\right|^2, \quad Z = \left.\frac{p}{\rho_0 c_0 u}\right|_{\text{interface}} = \Re + iX, \tag{1}$$

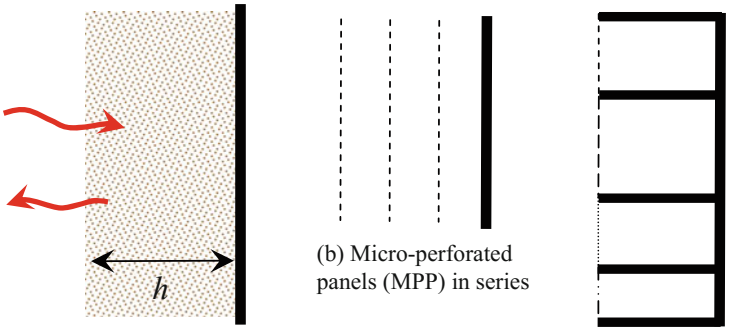

Fig. 1 Illustration of the absorption of normal incident sound by **a** a layer of sound absorption material (SAM) of depth h, **b** micro-perforated panels (MPP) in series and **c** in parallel

where Z is the interface impedance normalized by the air impedance $\rho_0 c_0$. For convenience, Z is decomposed into resistance $\mathfrak{R}$ (real part) and reactance X (imaginary part). Perfect sound absorption, $\alpha = 1$, requires $Z = 1$ or

$$Z = 1: \quad \mathfrak{R} = 1, \quad X = m\bar{\omega} - K/\bar{\omega} = 0 \rightarrow m = K = 0, \tag{2}$$

where m and K are the normalized system mass and stiffness, respectively, and

$$\bar{\omega} = \omega h / c_0 \tag{3}$$

is the dimensionless angular frequency. For the benchmark absorber shown in Fig. 1a, the interface impedance is approximated as follows

$$Z = \frac{\bar{\rho}_{sam}\bar{c}_{sam}}{i\tan(\bar{\omega}/\bar{c}_{sam})} \overset{\cot x \approx x^{-1} - x/3}{\longrightarrow} Z \approx i\left(\frac{\bar{\rho}_{sam}\bar{\omega}}{3} - \frac{\bar{\rho}_{sam}\bar{c}_{sam}^2}{\bar{\omega}}\right), \tag{4}$$

where $\bar{\rho}$ and $\bar{c}$ are the complex density and speed of sound normalized by the air density ρ_0 and speed of sound c_0, respectively, subscripts 'sam' denote sound absorption material, for which the classic Delany and Bazley [2] model is used

$$\begin{aligned} \bar{\rho}_{sam}\bar{c}_{sam} &= 1 + 0.057E^{-0.754} - i \times 0.087E^{-0.732}, \\ \bar{c}_{sam}^{-1} &= 1 + 0.098E^{-0.7} - i \times 0.189E^{-0.595}, \quad E = \rho_0 f / R_f. \end{aligned} \tag{5}$$

Here, R_f is the flow resistivity and parameter E should fall within the range of 0.01 and 1.0 for the empirical formulas to be reliable.

In Eq. (4), the decomposition into real and imaginary parts gives

$$\begin{aligned} \mathfrak{R} &= \mathrm{Re}(Z) = \mathrm{Im}\left(\bar{\rho}_{sam}\bar{c}_{sam}^2\right)/\bar{\omega} - \frac{1}{3}\mathrm{Im}(\bar{\rho}_{sam})\bar{\omega} \\ m &= \mathrm{Re}(\bar{\rho}_{sam})/3, \quad K = \mathrm{Re}\left(\bar{\rho}_{sam}\bar{c}_{sam}^2\right). \end{aligned} \tag{6}$$

For a cavity of pure air, the normalized mass is $m = 1/3$, which in dimensional sense means that one third of the mass of the air column in the cavity is vibrating with the interface. The system stiffness of $K = 1$ means a spring constant of $\rho_0 c_0^2 / h$ for an interface of unit area.

In a real system, the frequency dependency of the interface impedance Z is complex. The resistance $\mathfrak{R}$ is frequency dependent, and the reactance X does not yield a constant mass m and constant stiffness K. For any frequency band of interest, a least-mean-square fit for the reactance X (as a function of frequency) is to be used to analyze the system properties. For a discrete set of frequencies, usually chosen in equal logarithmic intervals with index $j = 1, 2, 3, \ldots, N$, the curve fitting is achieved as follows

$$\begin{bmatrix} m \\ K \end{bmatrix} = \begin{bmatrix} \sum_{j=1}^{N} \bar{\omega}_j^2 & -N \\ N & -\sum_{j=1}^{N} 1/\bar{\omega}_j^2 \end{bmatrix}^{-1} \begin{bmatrix} \sum_{j=1}^{N} X_j \bar{\omega}_j \\ \sum_{j=1}^{N} X_j/\bar{\omega}_j \end{bmatrix}. \tag{7}$$

Note that m and K are dependent on the choice of frequencies and caution must be exercised to interpret the results. When a set of system parameters are thus obtained, a resonant frequency may be obtained as $\bar{\omega} = \sqrt{K/m}$ which is easily translated into a dimensional frequency of $\bar{\omega} c_0/(2\pi h)$ in Hertz.

For all examples presented in this study, the frequency range and the absorber depth are chosen below

$$f \in [100,\ 1000]\ \text{Hz}, \quad h = 0.05\ \text{m}. \tag{8}$$

Figure 2a compares the sound absorption performance for three absorbers: SAM absorber, a single MPP and three MPPs in series, with design parameters given in the figure caption, while the legends (for all sub-figures) are given in Fig. 2c where there is more space for labels. The performance of SAM (solid line) is clearly poor at low frequencies and the same is true for the MPP in series (labelled as MPP-3). Note that the choice of $R_f = 5000\,\text{Pa}\cdot\,\text{s/m}^2$ is made on the basis of achieving some absorption in the low frequency region and an increase of R_f can easily raise the absorption coefficient towards 1 kHz but further suppress the low-frequency absorption. In fact, a systematic optimization scheme was used but the details are not described here for brevity. The main observation here is that the SAM performance is similar to that of MPP-3 (dotted line). The latter consists of 3 layers of MPP, equally spaced over the depth h. It must be cautioned that such panels will be rather expensive to make due to the very small aperture size (0.2 mm) and high perforation ratio specified. The purpose of the comparison is to show that MPPs can indeed achieve the same performance of the porous material but it would be rather expensive. The formulas of Maa [4] are used for the single-aperture impedance (denoted by subscripts '1')

$$\begin{aligned} Z_1 &= \mathfrak{R}_1 + iX_1, \quad \mathfrak{R}_1 = \frac{32\nu t}{c_0 d^2}\left[\left(1 + \frac{K_1^2}{32}\right)^{1/2} + \frac{\sqrt{2}}{32} K_1 \frac{d}{t}\right], \\ X_1 &= \frac{\omega}{c_0} t\left[1 + \left(1 + \frac{K_1^2}{2}\right)^{-1/2} + 0.85\frac{d}{t}\right], \quad K_1 = d\sqrt{\frac{\omega}{4\nu}}, \end{aligned} \tag{9}$$

where d is the aperture diameter, t is the panel thickness, $\nu = 1.5 \times 10^{-5}\,\text{m}^2/\text{s}$ is the kinematic viscosity of air, K_1 is the ratio of diameter to the boundary layer thickness. The panel impedance is Z_1/σ, where σ is the perforation ratio, while the interface impedance is $Z_1/\sigma - i\cot(\bar{\omega})$ from which the absorption coefficient is calculated according to Eq. (1).

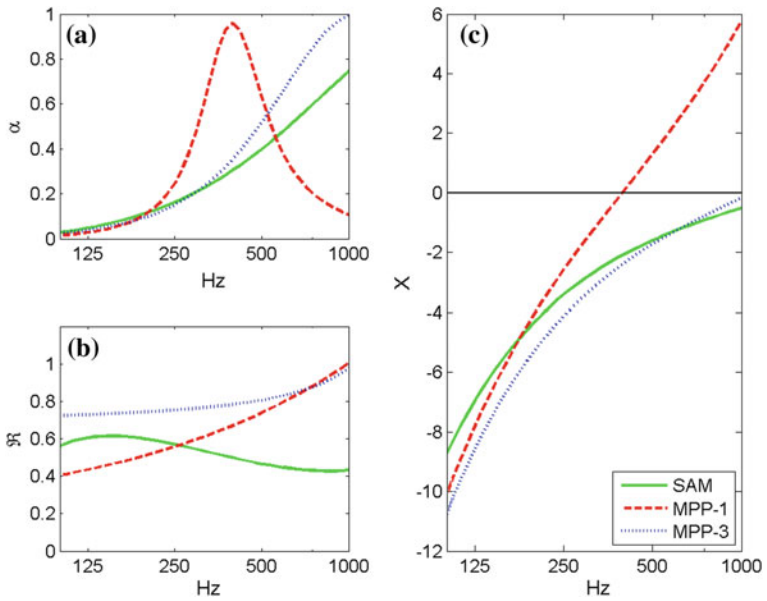

Fig. 2 Sound absorption by perforated panels: single vs a series of panels and comparison with SAM. **a** Absorption coefficients. **b** Resistance. **c** Reactance. The SAM has $R_f = 5000\,\text{Pa} \cdot \text{s/m}^2$; the single MPP resonator has a panel thickness of 0.5 mm, an aperture diameter of 1 mm, and a perforation ratio of 0.4%. The panels in MPP-3 configuration also have a thickness of 0.5 mm, all with an aperture diameter of 0.2 mm, and a perforation ratio of 4%

The dashed-line in Fig. 2a is for the single-MPP absorber with an aperture diameter of 1 mm, and a perforation ratio of $\sigma = 0.4\%$. Here, the very low ratio of σ is chosen in order to amplify (by the factor of σ^{-1}) the grossly inadequate resistance yielded by the aperture diameter of 1 mm. The consequence of such a low perforation ratio is that it also amplifies the virtual mass embedded in X_1. The curve-fitting by Eq. (6) gives $m = 7.58$, $K = 1.0$. The resonance frequency is 392.8 Hz. The high value of mass (compared with the natural cavity acoustic mass of $m = 1/3$) results in a performance drop above the resonance frequency.

Figure 2b shows the resistance for the three configurations. The ideal value of $\mathfrak{R}$ is unity, and the three curves are not too far from that. Figure 2c shows the reactance. The resonance of the single-MPP produces $X = 0$ around 392.8 Hz, while the curves for the SAM and MPP-3 configurations are similar.

As a summary, the following may be said. (i) The performance of the SAM absorber can be matched by MPPs in series, but the panels would be expensive to make. (ii) The single-MPP resonator can be designed to provide a fairly complete absorption at a single frequency and its poor performance elsewhere is caused by the resistance amplification by a low perforation ratio. (iii) Significant sound absorption below around 500 Hz is difficult to achieve by these three configurations.

3 Parallel Sound Absorber

Figure 1c illustrates the parallel absorber which was also reported by Wang and Huang [5] using cavities of various depths. In the current study, a uniform depth of h is used but the summation of acoustic admittance remains unchanged,

$$\frac{1}{Z} = \sum_j \frac{A_j}{Z_{1j}/\sigma_j - i\cot\bar{\omega}}, \quad \sum_j A_j = 1, \tag{10}$$

where A_j is the fraction of the interface area allocated to resonator j. Note that the results predicted by this equation may differ somewhat from a full numerical simulation (such as by Comsol) as the latter takes full account of the inter-resonator coupling which is typically adding virtual mass to the system. Such effects can easily be absorbed by the adjustment of the perforation ratios and are not discussed in detail here. However, the fundamental difference between the parallel arrangement in Fig. 1c and the series arrangement in Fig. 1b deserves some discussions.

The impedance of the series arrangement is a simple addition, while that of the parallel one is the summation of admittance. For the simplest case of two resonators with equal interface area,

$$Z_1 = \mathfrak{R}_1 + iX_1, \quad Z_2 = \mathfrak{R}_2 + iX_2, \quad A_1 = A_2,$$

the overall interface impedance is calculated as follows,

$$Z = 2\frac{Z_1 Z_2}{Z_1 + Z_2} = 2\frac{(\mathfrak{R}_1\mathfrak{R}_2 - X_1X_2) + i(\mathfrak{R}_1X_2 + \mathfrak{R}_2X_1)}{\mathfrak{R}_1 + \mathfrak{R}_2 + i(X_1 + X_2)}.$$

For a frequency between the two resonances where $X_2 = -X_1$, and assuming $\mathfrak{R}_1 = \mathfrak{R}_2$, the following interface impedance is obtained

$$Z = \frac{\mathfrak{R}_1^2 + X_1^2}{\mathfrak{R}_1}.$$

which is purely real. The reactance X_1 is transformed into resistance and it can be much larger than the resistance in each resonator, $|X_1| > \mathfrak{R}_1$ if the two resonance frequencies of the two resonators are far apart. The mechanism for such reactance-to-resistance transformation is explained as follows. When there is no resistance, $\mathfrak{R}_1 = \mathfrak{R}_2 = 0$, any acoustic pressure will drive particle velocities of opposite signs and they sum up to zero total volume flux,

$$u_1 = p/(iX_1), \quad u_2 = p/(iX_2), \quad u_1 + u_2 = 0,$$

as the two resonators form a new resonator, with the first (with lower own resonance frequency) playing the role of mass and the second playing the role of a spring, $X_1 > 0, \quad X_2 = -X_1 < 0$. This inter-resonator resonance is only curtailed

by the resistance $\Re_1 > 0$ which leads to $u_1 + u_2 \neq 0$. The net volume flux thus derived is out of phase with the resistance effect itself and is in-phase with the reactance of the individual resonator.

Figure 3 compares the performance of such a parallel absorber (with 10 resonators) with SAM. Figure 3a shows that an absorption coefficient near 0.5 is possible for frequencies ranging from 100 Hz to 1 kHz (dashed line for the parallel absorber) while the SAM absorber (solid line) can only reach such performance beyond around 500 Hz. The broad bandwidth for the parallel absorber is particularly significant.

However, the resistance data shown in Fig. 3b reveals that the parallel absorber (dashed line) has very high resistance (around 5.0) derived from the component reactance, while the SAM resistance is much closer to the ideal value of $\Re = 1$. Note that this level of resistance is about 4.2 times as high as the average resistance if all the panels were arranged in series. This again proves that the resistance is mainly derived from the reactance of individual resonators. In plain physics, it means that the velocity of the inter-resonator flow is so large that the system resistance is greatly amplified. Details of inter-resonator particle flow were analyzed by Wang and Huang [5] although the frequency bandwidth covered by that study

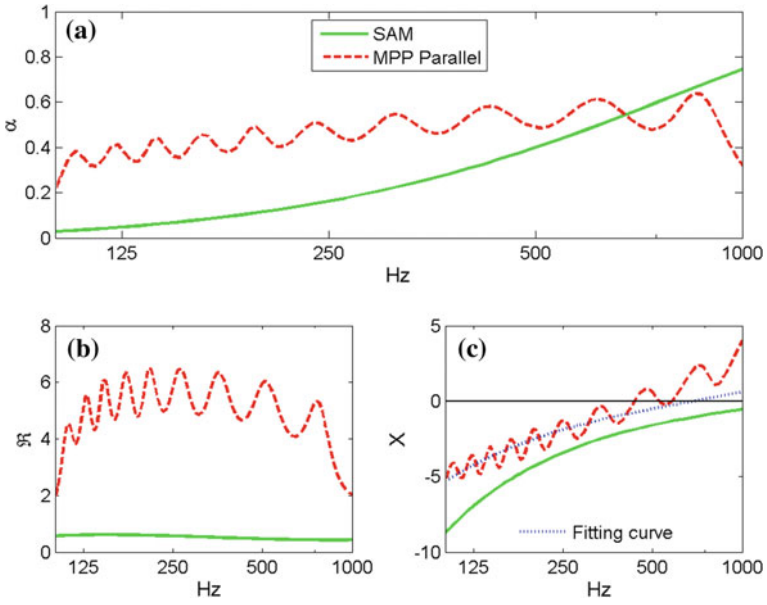

Fig. 3 Parallel MPP array compared with porous medium absorber. **a** Absorption coefficient. **b** Resistance. **c** Reactance. The SAM absorber has $R_f = 5000\,\text{Pa} \cdot \text{s/m}^2$. The parallel absorber of 10 MPPs has an A_p ranging from 0.05 to 0.123, and an aperture diameter from 0.58 to 4 mm

was not as large as in the current example. In this example, this high value of resistance from the parallel absorber is the reason why the absorption coefficient cannot rise above 0.5, unlike the single-resonator performance shown in Fig. 2a as the dashed line.

The reason why the broadband performance in Fig. 3a is possible in the first place is due to the fact that the inertia from one resonator is balanced by the spring from another ($X_1 > 0,\ X_2 < 0$). The cancellation of reactance among the resonators is best illustrated by the system stiffness determined by the least-mean-square fit which is shown as the dotted line in Fig. 3c. This curve is closer to the resonance condition of $X = 0$ than the SAM absorber (solid curve). For the particular example, the system parameters are $m = 1.2628,\ K = 0.5054$. Compared with the single-MPP resonator with $m = 7.58$, the parallel absorber has a rather low system mass. In terms of the more critical parameter of system stiffness, the value is nearly half of the simple cavity. In other words, the effective cavity size is nearly doubled by the parallel arrangement.

4 Advanced Concepts of System Mass and Stiffness Reduction

All configurations analyzed so far are purely mechanical and passive. In such a mechanical system mass can only be added, and it is most easily added by having a perforated panel of low perforation ratio. However, the fact that the parallel resonator with reactance shown in Fig. 3c has such a low system mass reveals that the inter-resonator coupling is able to take away inertia (namely negative dynamic mass) instead of adding to it. The exact mechanism by which this is achieved is complex, but it is likely that the phase angle change associated with the damping is involved. The other known example of negative dynamic mass was revealed by Huang [3]. The page limit here does not allow essential details to be reproduced but a brief summary of physics is necessary. When a flush-mounted piston vibrates on one duct wall, the baffling effect by the opposite duct wall introduces an image source which also radiates to the real piston surface which modifies the radiation impedance of the real piston. The fact that the waves from the image source travel a distance twice the duct height implies a time delay for the damping effect; the wave pressure being a damping term as the product of pressure and velocity carries power. The delayed damping term brings negative dynamic mass, as shown below,

$$\Re u_p(t-\Delta t) = \Re u_p e^{-i\omega\Delta t} \approx \Re u_p - \Re \Delta t\ du_p/dt,$$

where u_p is the piston vibration velocity, $\Delta t = 2h/c_0$ is the time delay, and the negative dynamic mass is simply $-\Re\Delta t$ as it gives rise to a force proportional to the piston acceleration du_p/dt. In the analysis of [3], the actual amount of negative mass is determined by the ratio of piston width to the duct height, and it can be

rather substantial for a wide piston. Having said these, the fact that the piston is assumed to vibrate at a uniform velocity implies a certain structural rigidity and hence structural mass. It is not easily conceivable that the negative mass effect would compensate for the extra structural mass brought by the piston.

The second advanced concept is the negative stiffness rendered by the magnetic force [3]. When a ferromagnetic material is placed in the field of a magnet, the material will be attracted to the magnet and the attraction force increases when the two objects are closer together, giving rise to negative stiffness which does not normally exist in pure mechanical systems. The concept was validated experimentally by Chiu et al. [1] who demonstrated clear resonance frequency shift towards lower frequencies. A very different approach of using a moving-coil loudspeaker diaphragm was proposed by Zhang et al. [6], Zhang and Huang [7] and it was shown that the magnetic force employed in such a design can effectively reduce the cavity stiffness and the cavity volume is estimated to be tripled by the use of the shunt circuit attached to the electromagnetic device.

5 Conclusions

For the purpose of control of sound waves, the acoustic impedance at the sound-absorber interface has two crucial components: system mass and stiffness. The latter controls the performance of the absorber at low frequencies and is determined mainly by the absorber volume. While electromagnetic forces can reduce system stiffness, a pure mechanical system of parallel array of Helmholtz resonators is also capable of significant stiffness reduction. In this study, an absorber designed by this approach delivers higher absorption coefficient from 100 Hz up to 1 kHz. However, the absolute level of the absorption coefficient is seen to be limited by the reactance-derived resistance.

In terms of the system mass, a single MPP resonator is seen to add too much mass that high frequency performance as an absorber is severely damaged. The array resonators, however, are found to yield only a moderate increase of system mass. Negative dynamic mass is also possible via delayed resistance but it remains to be seen if such mechanism can be used to form a practical device.

Acknowledgements The author gratefully acknowledges the funding support from the Department of Science and Technology of Zhejiang Province, China.

References

1. Chiu YH, Cheng L, Huang L (2006) Drum-like silencers using magnetic forces in a pressurized cavity. J Sound Vib 297:895–915
2. Delany M, Bazley E (1970) Acoustical properties of fibrous absorbent materials. Appl Acoust 3:105–116

3. Huang L (2000) A theory of reactive control of low-frequency duct noise. J Sound Vib 238 (4):575–594
4. Maa DY (1998) Potential of microperforated panel absorber. J Acoust Soc Am 104:2861–2866
5. Wang CQ, Huang L (2011) On the acoustic properties of parallel arrangement of multiple micro-perforated panel absorbers with different cavity depths. J Acoust Soc Am 130(1):208–218
6. Zhang YM, Chan YJ, Huang L (2014) Thin broadband noise absorption through acoustic reactance control by electro-mechanical coupling without sensor. J Acoust Soc Am 135 (5):2738–2745
7. Zhang YM, Huang L (2017) Electroacoustic control of Rijke tube instability. J Sound Vib 409:131–144